Six-Phase PMSM Drive Inverter Testing on a High Performance Power Hardware-in-the-Loop Testbed

Yasser Rahmoun, Patrick Winzer, Alexander Schmitt, Horst Hammerer
AVL SET GmbH
Franz-Josef-Spiegler-Str. 5
D- 88239 Wangen/Allgäu
Phone: +49 (0) 7522 91609-0
Fax: +49 (0) 7522 91609-299
Email: Yasser.Rahmoun@avl.com
URL: https://www.avl-set.com/

Keywords

≪Power Hardware-in-the-Loop≫, ≪Six-phase PMSM≫, ≪FEA≫, ≪Inverter testing≫, ≪Electrical machine emulator≫

Abstract

This paper presents for the first time a six-phase Power Hardware-In-the-Loop (PHIL) testbench, featuring electromagnetic effects such as magnetic coupling and spatial harmonics. The proposed PHIL testbed can be used for testing six-phase Permanent Magnet Synchronous Machine (PMSM) drive inverters for electric vehicles under realistic operation conditions. This paper describes the developed six-phase PMSM model and its parameterization, as well as the structure of the PHIL testbed. Finally, measurements and simulation results are compared and illustrated.

Introduction

Modern drive inverters of electric vehicles are becoming increasingly more complex; however, the development time and costs must be reduced. This conflict of objectives can only be solved using new development methods combined with new dedicated development tools for each component of the electric vehicle. This allows the parallel development of the components and consequently accelerates the complete development process of the vehicle [1].

Drive inverter testing on conventional testbeds (see Fig. 1) has a multitude of limitations, and therefore new tools are required. One of these limitations is that the tests can be only conducted when the real motor is already available, which is usually not the case as the motor must be developed simultaneously with the inverter. Moreover, fabrication tolerances of the electric motor lead to varying behavior of the Unit Under Test (UUT) on different motor testbeds at identical operation conditions, which make the tests on these testbeds not 100% reproducible.

To overcome the afore-mentioned limitations and to cope with the new test demands of the e-mobility industry, Power Hardware-in-the-Loop (PHIL) testbeds (see Fig. 2) are often employed. With these kind of testbeds drive inverter testing can start at a very early development stage even if the real motor is still not available. The reason behind this is that PHIL testbeds are capable of emulating electric motors based on their parameters, which can be either measured or calculated by means of Finite Element Analysis (FEA). Furthermore, PHIL tests are 100% reproducible, since firstly, the onetime measured or calculated parameters of an e-motor can be used to parametrize multiple testbenches and secondly, the tolerances of such testbeds are only determined by the accuracy of the used data acquisition. Therefore, the PHIL testbed solves some critical issues by the testing of drive inverters and dramatically accelerates their

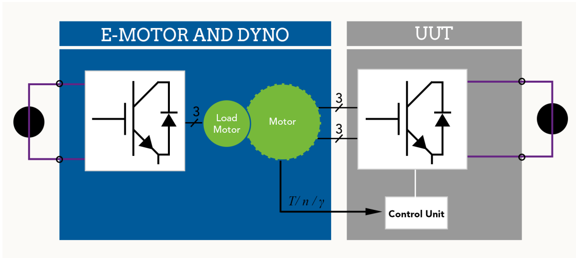

Fig. 1: Conventional testbed for six-phase inverters.
T is the torque, n is the mechanical rotor speed and γ is the mechanical rotor position.

development process. In general, a PHIL testbed comprises an Electrical Machine Emulator (EME) and two Power Supply Units (PSU) for both EME and UUT (see Fig. 2). The EME, which is the dominant part of the testbed, consists of the following three main components [2]:

1. A real-time processing system, which calculates the physical behavior of the emulated machine in real time based on its electrical and mechanical models.
2. A high switching frequency emulation converter, which imitates the electrical behavior of the machine in real time.
3. An ohmic inductive coupling network, which ensures a control path between the emulation converter and inverter.

The EME is supplied by a galvanically isolated DC PSU as the real machine windings are also galvanically isolated [3] [4].

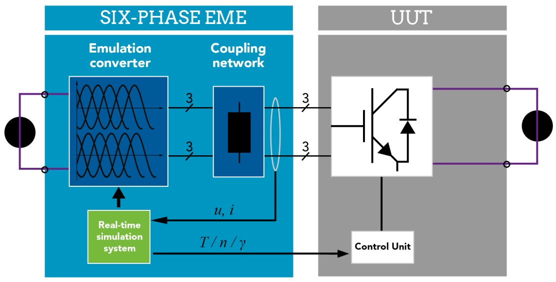

Fig. 2: PHIL testbed for six-phase inverters.
u is the measured line voltages and i is the measured phase currents.

Since the benefits of PHIL are not limited to a specific machine type, it can be applied to six-phase Permanent Magnet Synchronous Machines (PMSM). This machine type is gaining more and more attention in the field of e-mobility. This is due to firstly, the redundancy in its design, which makes it more reliable than the three-phase PMSM as it has two galvanically isolated stator winding systems and can continue to deliver power even if one of its stator winding systems fails. This is an important safety feature for autonomous driving vehicles, where the autonomous driving system can still get the vehicle off the road in the case of such faults [5]. Secondly, the six-phase PMSM has minor flux linkage harmonics in comparison with the three-phase PMSM and therefore, it is quieter, has better efficiency and has better torque quality [6]. Finally, the inverters of six-phase PMSM drives can be designed for either half the voltage or half the current at a given motor output power as compared to three-phase PMSM drive inverters, thereby potentially achieving cost or performance advantages [6].

On the other hand, the six-phase PMSM is more complex and needs a more sophisticated control scheme, because of the coupling between its stator winding systems. To overcome these drawbacks and to cover the test demand of six-phase traction inverters a high performance six-phase PHIL testbed was developed.

The goal of this contribution is to demonstrate the ability of the developed six-phase PHIL testbench to correctly emulate the highly sophisticated electromagnetic characteristics of a six-phase PMSM and finally to be used to test and evaluate the control scheme of a six-phase drive inverter. In the following section a theoretical six-phase PMSM electrical model is obtained. After that, the six-phase PMSM design is discussed and FEA data is derived. The subsequent section explains the developed six-phase PHIL testbed structure. Finally, real measurements of the emulated six-phase PMSM driven by a test inverter are presented and compared to simulation results.

Theoretical Description of the Emulated Six-Phase PMSM

Modeling of the Six-Phase PMSM in dq Domain

The six-phase PMSM is modeled in dq domain to simplify and decrease the calculation efforts of the model. It consists of two identical, galvanically isolated but magnetically coupled three phase systems. The modeled six-phase PMSM has a phase displacement $\alpha_{s1,s2}$ between its two stator winding systems and the star points of the two systems are not connected. Fig. 3 and Fig. 4 represent the six-phase PMSM equivalent circuits in UVW and dq domains respectively.

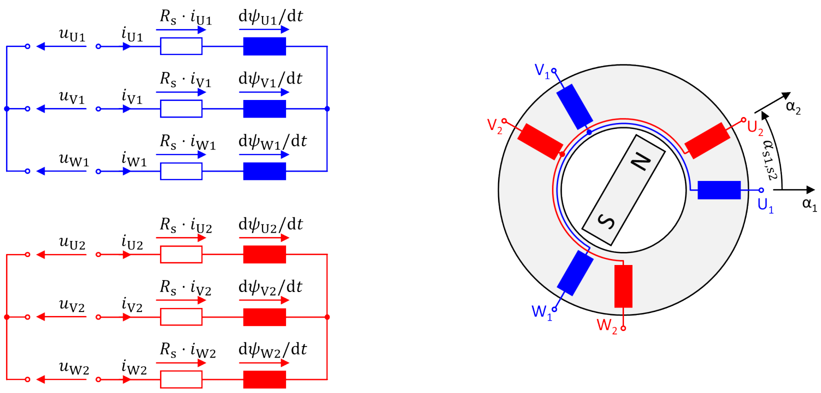

Fig. 3: Six-phase PMSM representation in UVW domain

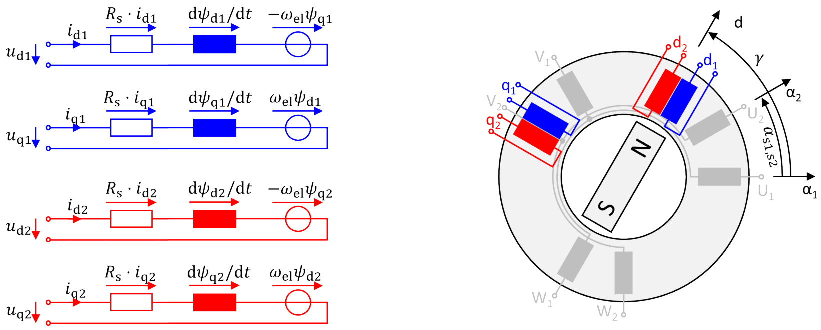

Fig. 4: Six-phase PMSM representation in dq domain

The voltage equations of the six-phase PMSM in UVW domain are given by Equation (1) and Equation (2), where R_s is the stator phase resistance, ψ is the flux linkage, u is the voltage, i is the current and t is the time.

$$\begin{aligned} u_{U1} &= R_s \cdot i_{U1} + \frac{d\psi_{U1}}{dt} \\ u_{V1} &= R_s \cdot i_{V1} + \frac{d\psi_{V1}}{dt} \\ u_{W1} &= R_s \cdot i_{W1} + \frac{d\psi_{W1}}{dt} \end{aligned} \qquad (1)$$

$$\begin{aligned} u_{U2} &= R_s \cdot i_{U2} + \frac{d\psi_{U2}}{dt} \\ u_{V2} &= R_s \cdot i_{V2} + \frac{d\psi_{V2}}{dt} \\ u_{W2} &= R_s \cdot i_{W2} + \frac{d\psi_{W2}}{dt} \end{aligned} \qquad (2)$$

By transforming the previously mentioned Equation (1) and Equation (2) in dq domain we get Equation (3).

$$\begin{aligned}
u_{\mathrm{d1}} &= R_{\mathrm{s}} \cdot i_{\mathrm{d1}} + \frac{\mathrm{d}\boldsymbol{\psi}_{\mathbf{d1}}}{\mathrm{d}t} - \omega_{\mathrm{el}} \cdot \boldsymbol{\psi}_{\mathbf{q1}} \\
u_{\mathrm{q1}} &= R_{\mathrm{s}} \cdot i_{\mathrm{q1}} + \frac{\mathrm{d}\boldsymbol{\psi}_{\mathbf{q1}}}{\mathrm{d}t} + \omega_{\mathrm{el}} \cdot \boldsymbol{\psi}_{\mathbf{d1}} \\
u_{\mathrm{d2}} &= R_{\mathrm{s}} \cdot i_{\mathrm{d2}} + \frac{\mathrm{d}\boldsymbol{\psi}_{\mathbf{d2}}}{\mathrm{d}t} - \omega_{\mathrm{el}} \cdot \boldsymbol{\psi}_{\mathbf{q2}} \\
u_{\mathrm{q2}} &= R_{\mathrm{s}} \cdot i_{\mathrm{q2}} + \frac{\mathrm{d}\boldsymbol{\psi}_{\mathbf{q2}}}{\mathrm{d}t} + \omega_{\mathrm{el}} \cdot \boldsymbol{\psi}_{\mathbf{d2}}
\end{aligned} \tag{3}$$

In this paper, bold print is used to highlight parameters which are dependent on the current components $i_{\mathrm{d1}}, i_{\mathrm{q1}}, i_{\mathrm{d2}}, i_{\mathrm{q2}}$ and the electrical rotor position γ_{el}. Equation (4) shows an example for $\boldsymbol{\psi}_{\mathbf{d1}}$.

$$\boldsymbol{\psi}_{\mathbf{d1}} = \psi_{\mathrm{d1}}(i_{\mathrm{d1}}, i_{\mathrm{q1}}, i_{\mathrm{d2}}, i_{\mathrm{q2}}, \gamma_{\mathrm{el}}) \tag{4}$$

In general, the derivatives of flux linkages noted in bold in Equation (3) can be written as total differentials. Equation (5) shows exemplarily the total differential of $\boldsymbol{\psi}_{\mathbf{d1}}$.

$$\frac{\mathrm{d}\boldsymbol{\psi}_{\mathbf{d1}}}{\mathrm{d}t} = \frac{\partial \boldsymbol{\psi}_{\mathbf{d1}}}{\partial i_{\mathrm{d1}}} \cdot \frac{\mathrm{d}i_{\mathrm{d1}}}{\mathrm{d}t} + \frac{\partial \boldsymbol{\psi}_{\mathbf{d1}}}{\partial i_{\mathrm{q1}}} \cdot \frac{\mathrm{d}i_{\mathrm{q1}}}{\mathrm{d}t} + \frac{\partial \boldsymbol{\psi}_{\mathbf{d1}}}{\partial i_{\mathrm{d2}}} \cdot \frac{\mathrm{d}i_{\mathrm{d2}}}{\mathrm{d}t} + \frac{\partial \boldsymbol{\psi}_{\mathbf{d1}}}{\partial i_{\mathrm{q2}}} \cdot \frac{\mathrm{d}i_{\mathrm{q2}}}{\mathrm{d}t} + \frac{\partial \boldsymbol{\psi}_{\mathbf{d1}}}{\partial \gamma_{\mathrm{el}}} \cdot \frac{\mathrm{d}\gamma_{\mathrm{el}}}{\mathrm{d}t} \tag{5}$$

The partial derivatives of $\boldsymbol{\psi}_{\mathbf{d1}}$ can be written as follows:

$$\frac{\partial \boldsymbol{\psi}_{\mathbf{d1}}}{\partial i_{\mathrm{d1}}} = \boldsymbol{L}_{\mathbf{d1,d1}}, \frac{\partial \boldsymbol{\psi}_{\mathbf{d1}}}{\partial i_{\mathrm{q1}}} = \boldsymbol{L}_{\mathbf{d1,q1}}, \frac{\partial \boldsymbol{\psi}_{\mathbf{d1}}}{\partial i_{\mathrm{d2}}} = \boldsymbol{L}_{\mathbf{d1,d2}}, \frac{\partial \boldsymbol{\psi}_{\mathbf{d1}}}{\partial i_{\mathrm{q2}}} = \boldsymbol{L}_{\mathbf{d1,q2}}, \frac{\partial \boldsymbol{\psi}_{\mathbf{d1}}}{\partial \gamma_{\mathrm{el}}} = \boldsymbol{\Lambda}_{\mathbf{d1,el}} \tag{6}$$

Where:
$\boldsymbol{L}_{\mathbf{d1,d1}}$ is the differential self inductance of d1 axis.
$\boldsymbol{L}_{\mathbf{d1,q1}}$ is the differential mutual inductance between d1- and q1-axes.
$\boldsymbol{L}_{\mathbf{d1,d2}}$ is the differential mutual inductance between d1- and d2-axes.
$\boldsymbol{L}_{\mathbf{d1,d2}}$ is the differential mutual inductance between d1- and q2-axes.
$\boldsymbol{\Lambda}_{\mathbf{d1,el}}$ is the differential electric angular dependency of the flux linkage in d1-axis.

In a similar manner it is possible to write the six-phase PMSM voltage equations given in Equation (3) as presented in Equation (7).

$$\begin{aligned}
u_{\mathrm{d1}} &= R_{\mathrm{s}} \cdot i_{\mathrm{d1}} + \boldsymbol{L}_{\mathbf{d1,d1}} \cdot \frac{\mathrm{d}i_{\mathrm{d1}}}{\mathrm{d}t} + \boldsymbol{L}_{\mathbf{d1,q1}} \cdot \frac{\mathrm{d}i_{\mathrm{q1}}}{\mathrm{d}t} + \boldsymbol{L}_{\mathbf{d1,d2}} \cdot \frac{\mathrm{d}i_{\mathrm{d2}}}{\mathrm{d}t} + \boldsymbol{L}_{\mathbf{d1,q2}} \cdot \frac{\mathrm{d}i_{\mathrm{q2}}}{\mathrm{d}t} + \omega_{\mathrm{el}}(\boldsymbol{\Lambda}_{\mathbf{d1,el}} - \boldsymbol{\psi}_{\mathbf{q1}}) \\
u_{\mathrm{q1}} &= R_{\mathrm{s}} \cdot i_{\mathrm{q1}} + \boldsymbol{L}_{\mathbf{q1,d1}} \cdot \frac{\mathrm{d}i_{\mathrm{d1}}}{\mathrm{d}t} + \boldsymbol{L}_{\mathbf{q1,q1}} \cdot \frac{\mathrm{d}i_{\mathrm{q1}}}{\mathrm{d}t} + \boldsymbol{L}_{\mathbf{q1,d2}} \cdot \frac{\mathrm{d}i_{\mathrm{d2}}}{\mathrm{d}t} + \boldsymbol{L}_{\mathbf{q1,q2}} \cdot \frac{\mathrm{d}i_{\mathrm{q2}}}{\mathrm{d}t} + \omega_{\mathrm{el}}(\boldsymbol{\Lambda}_{\mathbf{el,q1}} + \boldsymbol{\psi}_{\mathbf{d1}}) \\
u_{\mathrm{d2}} &= R_{\mathrm{s}} \cdot i_{\mathrm{d2}} + \boldsymbol{L}_{\mathbf{d2,d1}} \cdot \frac{\mathrm{d}i_{\mathrm{d1}}}{\mathrm{d}t} + \boldsymbol{L}_{\mathbf{d2,q1}} \cdot \frac{\mathrm{d}i_{\mathrm{q1}}}{\mathrm{d}t} + \boldsymbol{L}_{\mathbf{d2,d2}} \cdot \frac{\mathrm{d}i_{\mathrm{d2}}}{\mathrm{d}t} + \boldsymbol{L}_{\mathbf{d2,q2}} \cdot \frac{\mathrm{d}i_{\mathrm{q2}}}{\mathrm{d}t} + \omega_{\mathrm{el}}(\boldsymbol{\Lambda}_{\mathbf{el,d2}} - \boldsymbol{\psi}_{\mathbf{q2}}) \\
u_{\mathrm{q2}} &= R_{\mathrm{s}} \cdot i_{\mathrm{q2}} + \boldsymbol{L}_{\mathbf{q2,d1}} \cdot \frac{\mathrm{d}i_{\mathrm{d1}}}{\mathrm{d}t} + \boldsymbol{L}_{\mathbf{q2,q1}} \cdot \frac{\mathrm{d}i_{\mathrm{q1}}}{\mathrm{d}t} + \boldsymbol{L}_{\mathbf{q2,d2}} \cdot \frac{\mathrm{d}i_{\mathrm{d2}}}{\mathrm{d}t} + \boldsymbol{L}_{\mathbf{q2,q2}} \cdot \frac{\mathrm{d}i_{\mathrm{q2}}}{\mathrm{d}t} + \omega_{\mathrm{el}}(\boldsymbol{\Lambda}_{\mathbf{el,q2}} + \boldsymbol{\psi}_{\mathbf{d2}})
\end{aligned} \tag{7}$$

Six-Phase PMSM Model Depths

Using Equation (7), three model depths are considered by the parameterization of the six-phase PMSM model, which are:

- Linear model
- Nonlinear model
- Nonlinear model, with spatial harmonics

Linear Model

The linear model considers just the magnetic coupling of stator winding systems (d1 ↔ d2 and q1 ↔ q2) and the potentially anisotropic geometry of a six-phase PMSM. In this model just the constant quantities for R_s, $L_\mathrm{d1,d1}$, $L_\mathrm{d1,d2}$, $L_\mathrm{q1,q1}$, $L_\mathrm{q1,q2}$ and ψ_PM are used to parameterize the model. By making use of the symmetry of the stator winding systems the quantities mentioned in Equation (8) can be also obtained.

$$\begin{aligned} L_\mathrm{d2,d2} &= L_\mathrm{d1,d1},\ L_\mathrm{d2,d1} = L_\mathrm{d1,d2} \\ L_\mathrm{q2,q2} &= L_\mathrm{q1,q1},\ L_\mathrm{q2,q1} = L_\mathrm{q1,q2} \end{aligned} \tag{8}$$

The flux linkages of the six-phase PMSM in this model are given by Equations (9).

$$\begin{aligned} \psi_\mathrm{d1} &= \psi_\mathrm{PM} + L_\mathrm{d1,d1} \cdot i_\mathrm{d1} + L_\mathrm{d1,d2} \cdot i_\mathrm{d2} \\ \psi_\mathrm{q1} &= L_\mathrm{q1,q1} \cdot i_\mathrm{q1} + L_\mathrm{q1,q2} \cdot i_\mathrm{q2} \\ \psi_\mathrm{d2} &= \psi_\mathrm{PM} + L_\mathrm{d2,d1} \cdot i_\mathrm{d1} + L_\mathrm{d2,d2} \cdot i_\mathrm{d2} \\ \psi_\mathrm{q2} &= L_\mathrm{q2,q1} \cdot i_\mathrm{q1} + L_\mathrm{q2,q2} \cdot i_\mathrm{q2} \end{aligned} \tag{9}$$

Nonlinear Model

The nonlinear model considers the nonlinear magnetic characteristic of iron (saturation) and the magnetic cross-coupling of d- and q-axes in addition to the linear model properties. In this model two 4-dimensional Lookup Tables (LUT) for each $\boldsymbol{\psi}_\mathbf{d1}$ and $\boldsymbol{\psi}_\mathbf{q1}$ (see Equation (10)) are used to parameterize the model, where $\boldsymbol{\psi}_\mathbf{d2}$ and $\boldsymbol{\psi}_\mathbf{q2}$ can be obtained from $\boldsymbol{\psi}_\mathbf{d1}$ and $\boldsymbol{\psi}_\mathbf{q1}$ basing on the symmetry of the stator winding systems.

$$\begin{aligned} \boldsymbol{\psi}_\mathbf{d1} &= \psi_\mathrm{d1}(i_\mathrm{d1}, i_\mathrm{q1}, i_\mathrm{d2}, i_\mathrm{q2}) \\ \boldsymbol{\psi}_\mathbf{q1} &= \psi_\mathrm{q1}(i_\mathrm{d1}, i_\mathrm{q1}, i_\mathrm{d2}, i_\mathrm{q2}) \end{aligned} \tag{10}$$

Nonlinear Model with Spatial Harmonics

The nonlinear model with spatial harmonics considers, in addition to the properties of linear and nonlinear models, the spatial harmonics effects. For the parameterization of this model two 5-dimensional LUTs for each $\boldsymbol{\psi}_\mathbf{d1}$ and $\boldsymbol{\psi}_\mathbf{q1}$ (see Equation (11)) are used, where $\boldsymbol{\psi}_\mathbf{d2}$ and $\boldsymbol{\psi}_\mathbf{q2}$ similarly to the nonlinear model can be obtained from $\boldsymbol{\psi}_\mathbf{d1}$ and $\boldsymbol{\psi}_\mathbf{q1}$ basing on the symmetry of the stator winding systems.

$$\begin{aligned} \boldsymbol{\psi}_\mathbf{d1} &= \psi_\mathrm{d1}(i_\mathrm{d1}, i_\mathrm{q1}, i_\mathrm{d2}, i_\mathrm{q2}, \gamma_\mathrm{el}) \\ \boldsymbol{\psi}_\mathbf{q1} &= \psi_\mathrm{q1}(i_\mathrm{d1}, i_\mathrm{q1}, i_\mathrm{d2}, i_\mathrm{q2}, \gamma_\mathrm{el}) \end{aligned} \tag{11}$$

Six-Phase PMSM Example

The used six-phase PMSM has been calculated by means of FEA. Its geometry has been derived from a three-phase PMSM geometry. The machine has buried Neodymium magnets in a U-shape, which yield anisotropic behavior. The iron saturation has been considered by the FEA. The machine's windings are distributed, in such way that there is one coil per phase and pole pair. Fig. 5a illustrates the FEA model

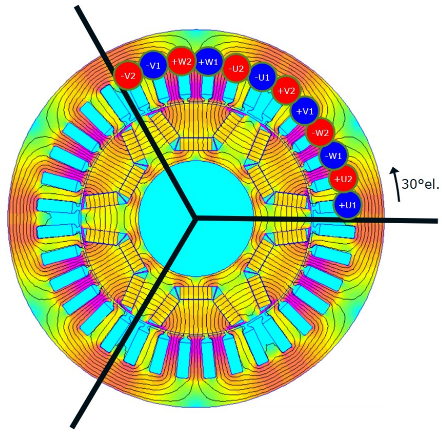

(a) FEA model of the used six-phase PMSM

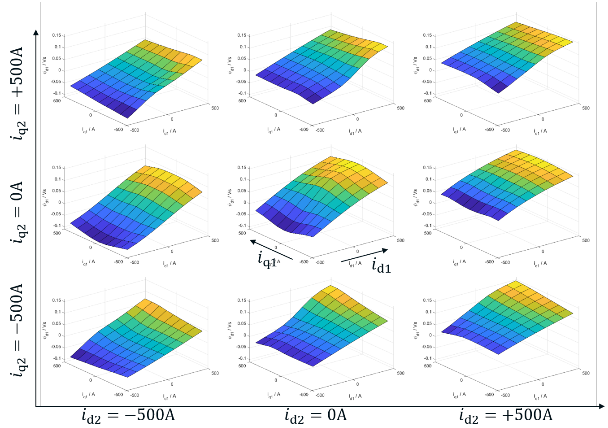

(b) $\psi_{d1}(i_{d1}, i_{q1}, i_{d2}, i_{q2}, \gamma_{el} = 0)$ of the used six-phase PMSM

Fig. 5: Used six-phase PMSM example

of the analyzed six-phase PMSM. The six-phase PMSM has a number of pole pairs $p = 3$, a stator phase resistance $R_s = 12m\Omega$ and a phase displacement $\alpha_{s1,s2} = 30°$.

The resulting flux linkage maps are presented in Fig. 5b, where it can be seen that the analyzed machine exhibits various electromagnetic effects such as saturation, d/q-cross coupling, inter-stator coupling and inter-stator d/q-cross coupling.

Fig. 6a shows the flux linkage in d1 axis as function to i_{d1}, i_{q1} and γ_{el}, whereas $i_{d2} = 0$ and $i_{q2} = 0$. Fig. 6b and Fig. 6c show the partial differential of ψ_{d1} with respect to i_{d1} and i_{q1} respectively. The flux linkage of the machine has an extra dependency on rotor position. Fig. 6d shows the dependency of ψ_{d1} on γel , which is the 5th dimension of the LUTs.

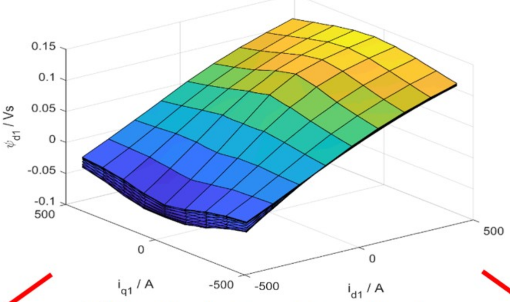

(a) $\psi_{d1}(i_{d1}, i_{q1}, i_{d2} = 0, i_{q2} = 0, \gamma_{el})$

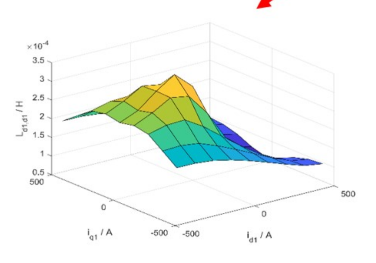

(b) $L_{d1,d1} = \frac{\partial \psi_{d1}(i_{d1}, i_{q1}, i_{d2}=0, i_{q2}=0, \gamma_{el}=0)}{\partial i_{d1}}$

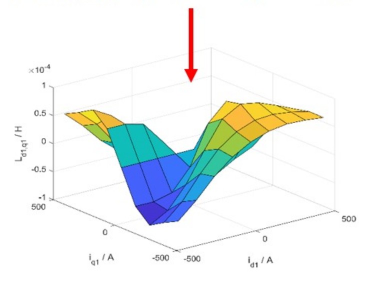

(c) $L_{d1,q1} = \frac{\partial \psi_{d1}(i_{d1}, i_{q1}, i_{d2}=0, i_{q2}=0, \gamma_{el}=0)}{\partial i_{q1}}$

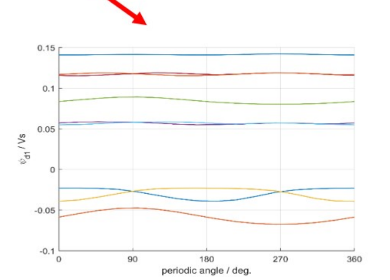

(d) $\psi_{d1}(i_{d1} = \{-500, 0, 500\}, i_{q1} = \{-500, 0, 500\}, i_{d2} = 0, i_{q2} = 0, \gamma_{el})$

Fig. 6: ψ_{d1} dependencies on i_{d1}, i_{q1} and γ_{el}

Six-Phase PMSM Emulator

Based on the obtained six-phase PMSM electrical model in dq domain (see Equation (7)) a numerical fixed point six-phase PMSM model (see Fig. 7) is developed and implemented in a Field Programable Gate Array (FPGA) to minimize dead times and achieve the highest possible model calculation frequency of 3.125 MHz (with the used FPGA). Within each calculation interval the electromagnetic equations are evaluated and an interpolation of the magnetic parameters' LUTs of up to five dimensions is executed. Furthermore, the FPGA model (see Fig. 7) calculates both three-phase set voltages, which have to be applied on the coupling network of each stator system very precisely and with a minimal dead-time to ensure the correct emulation of the six-phase PMSM phase currents in both stator systems.

To ensure a precise and fast realization of the two three-phase set voltages calculated by the FPGA model, two three-phase high switching frequency multilevel inverters (one for each stator system) are employed and the multilevel inverters switching frequency is set to 800 kHz. The two multilevel inverters are connected to two ohmic inductive coupling networks (one for each stator system), which ensure a control path between the two multilevel inverters and the inverter under test.

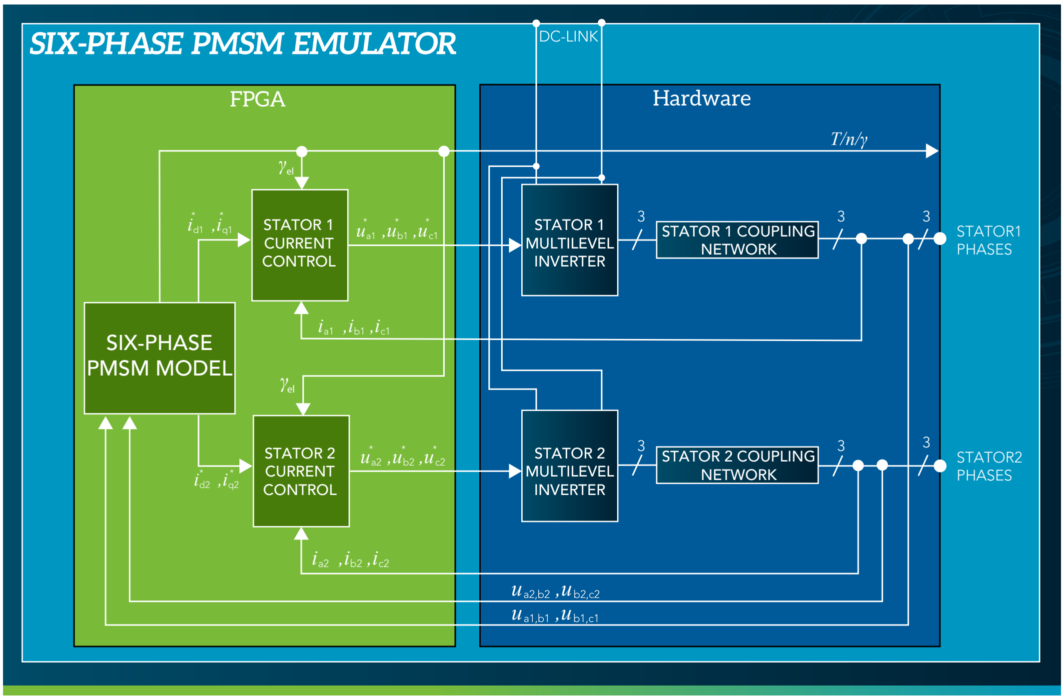

Fig. 7: Six-phase emulator functional diagram

Results

To prove the emulation quality of the developed six-phase PMSM testbench (see previous chapters) a series of tests was performed on the PHIL testbed (see Fig. 2) using the afore-mentioned parametrization for the nonlinear model with spatial harmonics. As a drive inverter, a six-phase PMSM drive inverter was utilized, which has a flux based predictive control scheme to drive the six-phase PMSM, derived from [7].

The results of the tests were then compared to simulation results of a MATLAB/Simulink® model, which represents the ideal case.

Back-EMF Test

In this test the emulated six-phase PMSM has no current flowing in its phases and the back EMF voltage amplitude is dependent on the machine permanent magnet flux and rotor speed. The voltage harmonics depend on how much the permanent magnet flux fluctuates as the machine rotates.

Fig. 8 shows the measured and simulated six-phase PMSM back-EMF line to line voltages of the first stator winding system at a rotor speed of 5000 RPM. The measured voltages are slightly filtered. Although the EME is predominantly a controlled current source (see Fig. 7), the back EMF matches the theoretical result well. The deviations between the measured and simulation results are due to the imperfection of the hardware.

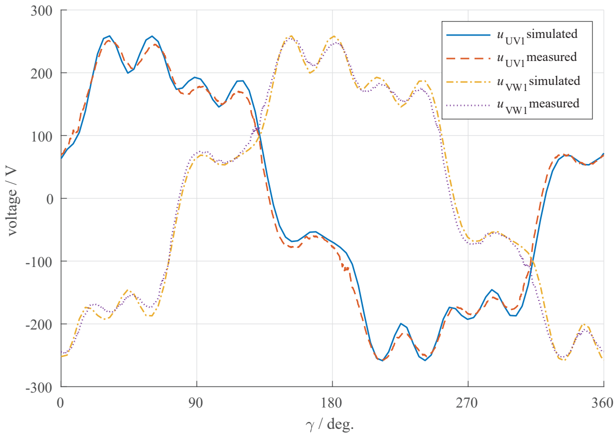

Fig. 8: Back-EMF voltage

Load Step Test

In order to present the capability of the emulator to precisely emulate the various electromagnetic characteristics of the six-phase PMSM in dynamic operation cases a dynamic current step in the q2 axis from 200 A to -200 A is performed on the PHIL testbed, while: $i_{\mathrm{q1\ set}}$ =200 A, $i_{\mathrm{d1\ set}} = -200A$ and $i_{\mathrm{d2\ set}} = -200A$. The current step in the q2 axis is delivered at a rotor speed of 1000 RPM. Fig. 9 demonstrates the measured and simulated currents of the six-phase PMSM in dq domain during the above-mentioned current step.

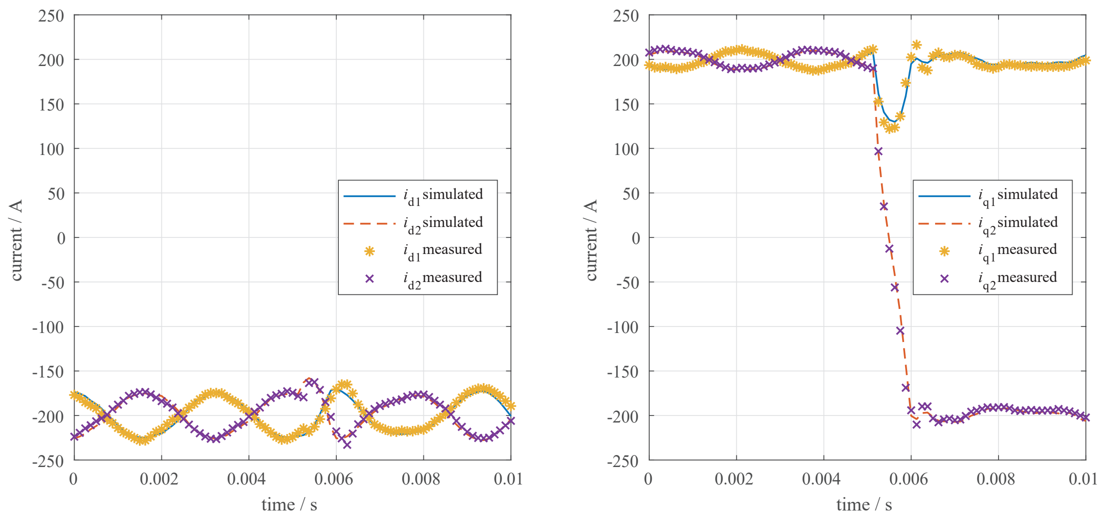

Fig. 9: Six-phase PMSM step response on q axis.
Note: Both measured and simulated results are sampled at 8 kHz sampling frequency, which is also the inverter switching frequency, hence it is not possible to see the current ripple of the inverter itself.

The results in Fig. 9 demonstrate that all magnetic effects of the six-phase PMSM, which are mentioned in the NLH model's properties, are covered by the developed six-phase PMSM testbed. The opposite phase of i_{d1} and i_{d2} respectively i_{q1} and i_{q2} is due to the 30° phase displacement between the two stator winding systems ($\alpha_{\mathrm{s1,s2}}$), which leads to a 180° phase shift in the dominating 6th order harmonics of the flux linkages.

Active Short Circuit Test

In this test, while the emulated six-phase PMSM runs in steady state and exhibits $i_{q1} = i_{q2} = 100A$ and $i_{d1} = i_{d2} = -100A$ at a rotor speed of 500 RPM, the six-phase inverter goes into safe state and applies an Active Short Circuit (ASC) on the 3 phases of each stator winding system at the same time. Fig. 10 shows the response of the emulated six-phase PMSM in this test.

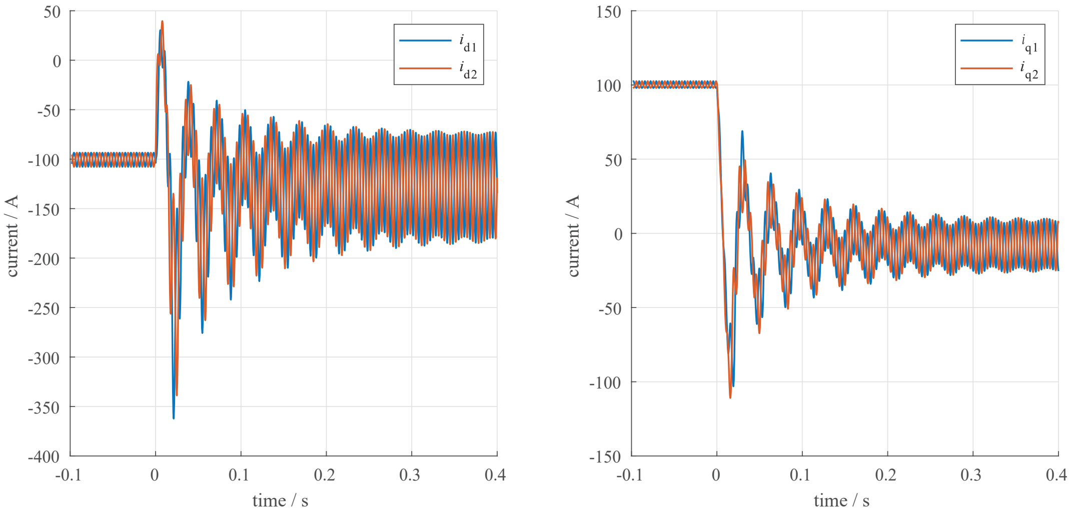

Fig. 10: Active short circuit test results (sampling rate 8 kHz)

In Fig. 11, the resulting currents in d- and q-axes are plotted against each other to show the course of the currents in both stator winding systems after the inverter applies the ASC. Fig. 11 shows that the inverter safe mode entering, at the previously mentioned operation point, could lead to phase overcurrents in the real machine, as the circle in the figure with the smaller radius represents its phase maximum current ($i_{\text{max real machine}}$). On the other hand, it is very important that the used PHIL testbed provides a high enough EME phase maximum current ($i_{\text{max EME}}$), represented by the circle with the greater radius, that it is able to emulate such high fault currents.

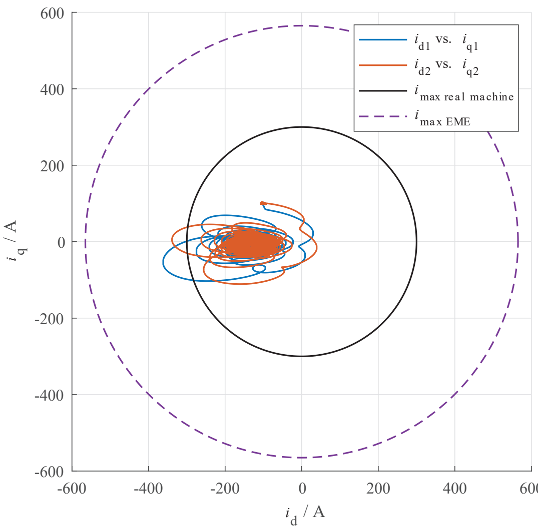

Fig. 11: Active short circuit test results in the $i_d - i_q$ plane (sampling rate 8 kHz)

Conclusion

In this contribution, a PHIL testbed for testing six-phase PMSM drive inverters has been proposed for the first time. The implemented PMSM model and its parameterization have been derived and discussed in detail, besides the structure of the proposed PHIL testbench.

The capability of the used PHIL testbed to emulate all relevant electromagnetic characteristics of the six-phase PMSM, along with the control scheme evaluation of a six-phase PMSM drive inverter have been then presented.

The test measurements have proved the high emulation quality of the developed PHIL testbench, which is due to the precise six-phase PMSM model and parameterization of the machine, the high calculation frequency of the FPGA-based machine model and the high dynamic emulation converter used to imitate the machine.

The measurements have also shown the ability of the used PHIL testbed to emulate fault scenarios, which permits the early identification of hardware limitations in the inverter and machine design.

With the proposed PHIL testbed, the development of inverters can be accelerated significantly, as many tests can be carried out even before the real motor exists using e.g. FEA data. Due to the automatization capability of the PHIL testbed, fast and reproducible test runs are possible.

References

[1] A. Schmitt, H. Hammerer, P. Winzer, and M. Schnarrenberger, "Drive inverter testing with virtual e-motors using power hardware-in-the-loop emulator concept," in AVL 8th International Symposium on Development Methodology, Nov. 2019.

[2] A. Schmitt, J. Richter, M. Braun, and M. Doppelbauer, "Power hardware-in-the-loop emulation of permanent magnet synchronous machines with nonlinear magnetics – concept & verification," in Proceedings of PCIM Europe, May 2016, pp. 393–400.

[3] A. Schmitt, M. Gommeringer, J. Kolb, and M. Braun, "A high current, high frequency modular multiphase multilevel converter for power hardware-in-the-loop emulation," in Proceedings of PCIM Europe, May 2014, pp. 1537–1544.

[4] A. Schmitt, M. Gommeringer, C. Rollbühler, P. Pomnitz, and M. Braun, "A novel modulation scheme for a modular multiphase multilevel converter in a power hardware-in-the-loop emulation system," in IECON - 41st Annual Conference of the IEEE Industrial Electronics Society, Nov. 2015, pp. 1276–1281.

[5] A. Kilic, J. Faßnacht, T. Shen, and C. Thulfaut, "Fehlertolerante Antriebsstränge für zukünftige Mobilität", MTZ-Motorteschnische Zeitschrift, Tech. Rep., 2019.

[6] E. Levi, R. Bojoi, F. Profumo, H. A. Toliyat and S. Williamson, "Multiphase induction motor drives - a technology status review," in IET Electric Power Applications, vol. 1, no. 4, pp. 489-516, July 2007, doi: 10.1049/iet-epa:20060342.

[7] P. Winzer, J. Richter and M. Doppelbauer, "Dynamic control of generalized electrically excited synchronous machines using predictive flux control," IECON 2016 - 42nd Annual Conference of the IEEE Industrial Electronics Society, Florence, 2016, pp. 2772-2777, doi: 10.1109/IECON.2016.7793666.